Desalination and Water Treatment
www.deswater.com

27 (2011) 255–267
March

1944-3994/1944-3986 © 2011 Desalination Publications. All rights reserved
doi: 10/5004/dwt.2011.2026

Modeling in desalination—electro-dialysis reversal

Maung Thein Myint[a,*], Abbas Ghassemi[a,b], Nagamany Nirmalakhandan[c]

[a]*Institute for Energy and the Environment, New Mexico State University, MSC WERC, P.O. Box 30001, Las Cruces, NM 88003, USA*
Tel. +575 646 2073; email: mmyint@nmsu.edu; mmyint2001@hotmail.com
[b]*Chemical Engineering Department, New Mexico State University, MSC WERC, P.O. Box 30001, Las Cruces, NM 88003, USA*
[c]*Civl Engineering Department, New Mexico State University, MSC 3CE, P.O. Box 30001, Las Cruces, NM, USA*

Received 16 May 2010; Accepted 25 July 2010

ABSTRACT

The first innovative model is developed in electro-dialysis reversal (EDR) desalination. First, theoretical limiting current density (LCD) determination is fitted and validated with four test-runs literature lab data. The goodness of fit and validation of LCD is statistically high with overall r^2 0.966 at $p < 0.001$. Second, a sensitivity analysis is done to study the most sensitive parameter in EDR with the LCD to its six modeling parameters; it was found that transport numbers of ions in membrane (t_{im}) and in solution (t_{is}) are rate limiting. Third, the model is constructed with emphases on LCD, concentration potential (CP), and total area of resistances of both membrane and solution to highlighting these two limiting parameters. Fourth, the model is fitted, verified, and validated with six different sets of both desalting energy and TDS in concentrate data from five literatures including 59 measured data points with five different feedwater characteristics. The values of five parameters ($t_{Ca^{++},m}$, $t_{Mg^{++},m}$, $t_{Na^{+},s}$, $t_{Ca^{+},s}$ $t_{Mg^{++},s}$) are generated from 30 model-runs. A new parameter, area resistance of solution, is found by model. Area resistance of solution increases with the increasing of mean-ions-resident time ($MIRT_c$) in concentrate of EDR in the same polar reversal interval; so as the desalting energy. The acids and anti-scalant adding in concentrate increases the area resistance of solution in model and increases desalting energy in pilot scale literature data. Literature data proves, there are not acids and anti-scalant adding requirement and no water leakage, if EDR is operated at $MIRT_c < 130$ min. By operating EDR at $MIRT_c < 130$ min, 3.2–31% of desalting energy can be saved, with the evidence of measured literature pilot scale desalting energy data, due to the lower area resistance of solutions in EDR, without requirement of adding acids and anti-scalant, and no water leakage.

Keywords: Acid; Anti-scalant; Concentration Potential; Limiting current density; Mean ions resident time in concentrate; Total area resistances of solution

1. Introduction

Electro-dialysis reversal (EDR) is invented for self-cleaning [1] by reversing the polarity and hydraulic streams. During the EDR reversing, the polarity switches in the electrodes which results in changing the chemical reaction within the electrode compartments. The cathode releases alkalinity resulting scaling; the anode electrode produces acid from the chemical reactions in Fig. 1. Because of the reversal, the scalants produced in the previous reversal can be cleaned by the acid which will be produced in the existing reversal. The acid environment in anode electrode can be optimized effectively to the lower pH by balancing the flushing rate which releasing out the chlorine and oxygen gas generated from the anode electrode compartment. The reversal in EDR gains four major benefits — destroys the polarization film three to four times an hour to prevent

*Corresponding author.

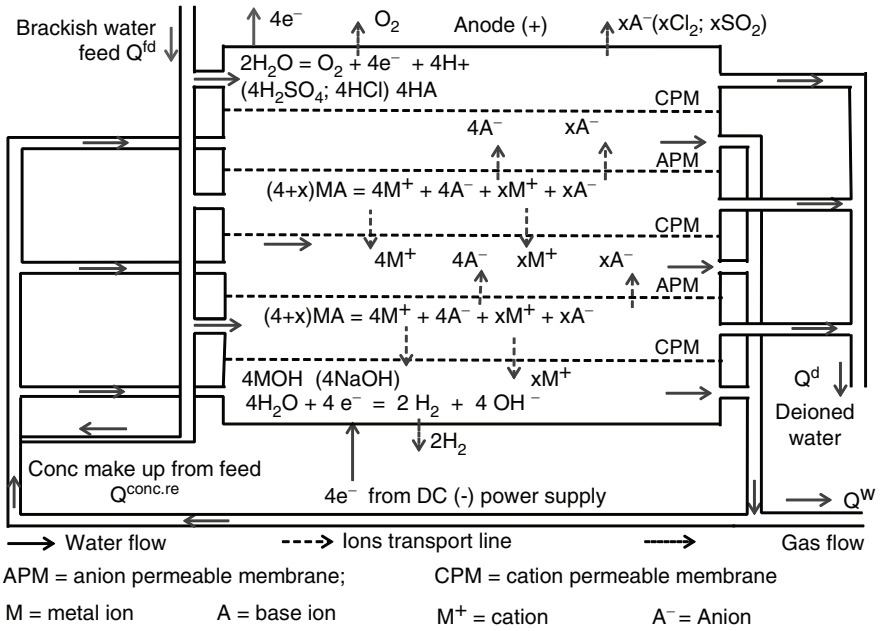

Fig. 1. Chemical reactions in EDR.

polarization scale; destroys newly precipitated scale or seeds of scale and washes them out to waste before they can block in membrane; minimizes slime formations on membrane surfaces from opposing the direction of colloidal particle movement; eliminates the whole complicated real problems resulting from the continuous injecting of non-environmental friendly acids and anti-scalant chemicals [1].

EDR has been successfully operating with the brackish ground water without any acids and any chemical addition in concentrate stream with Langelier saturation index (LSI) +2.16 (in field scale; [2,3]) and LSI + 2.4 (in lab; [4]) with low mean-ions residence time in concentrate ($MIRT_c$). EDR is branded or gradually known for its excellent ability to desalt SO_4^{2-} dominated brackish ground water. Chemical and acids additions can effectively control $CaCO_3$ scaling but less effectively $CaSO_4$ scaling [2]. However, due to its polarization reversal frequency to clean up the scaling especially from calcium sulfate, EDR can operate without any chemical addition with *calcium sulfate* levels greater than *saturation*; the upper design limit for calcium sulfate level is 150% [5] or 175% [1] or 400% [4] of $CaSO_4$ saturation in which there is no chemical addition requirement for cleaning [2,5].

To gain the higher water recovery rate and to reduce the amount of waste concentrate from EDR and to maintain the equal pressure and velocity between concentrate and dilute streams, the concentrate from outlet of the concentrate stream is *currently recycled* back into the inlet of the concentrate stream [1]; the unwelcomed ions are also recycled back into concentrate stream along with concentrate recycling. Therefore, the unwelcomed ions are eventually built-up and condense in the concentrate stream; scaling along the surface of membrane will begin if the Langelier saturation index (LSI) is greater than +2.2 [1,6] or $MIRT_c > 130$ [7]. The operation of LSI in concentrate stream can be increased to +2.4 with low mean resident time [4] or $MIRT_c < 130$ min [7]. These ions building-up in concentrate stream and in the surface of membrane facing to the concentrate may obstruct ions transport from dilute to concentrate passing through the membrane. Acid and anti-scalant chemicals are normally injected in concentrate steam of EDR operation to get away of the scalants from scaling.

For the higher water recovery rate, the amount of the concentrate recycle has to be much higher than the amount of waste stream [7]. This results in the higher *mean-ion retention time* in the concentrate ($MIRT_c$) [7]; the higher the $MIRT_c$ is, the more opportunities for membrane to damage and to shorten the life time from $CaSO_4$ and $CaCO_3$ scalants [2,8]. The more the ions are retained in the concentrate stream, the higher the concentrate potential exists between the concentrate and dilute streams [9]. The higher concentrate potential requires the higher power current to attach the ions from dilute steam to migrate into the denser concentrate stream. This denser ion concentration in concentrate stream increases the boundary layer in concentrate side of membrane, therefore *hinder* transport # of ions in membrane (t_{im}) and enhance transport # of ions in solution (t_{is}) [10].

There are three criteria required for the scale-forming material to cause problems in the membrane surface of the

concentrate stream of EDR—species, dose, and contact time. There will be no scaling formed, if one of these is not high enough. The reasons for the EDR to operate in LSI < +2.11 are to reduce both the species and the concentrations that have potential harmful to the membrane in concentrate stream. Contact exposure time or the mean-ion retention time (MIRT) can also be reduced by less recirculation or recycling to a level in which MIRT is not long enough for scalants ($CaSO_4$, $MgCO_3$, and $CaCO_3$) to create problems [4]. These reductions may *enhance* the transport number of ions in membrane (t_{im}) and in solution (t_{is}) for boosting the mass transfer coefficient, k. $MIRT_c$ is calculated as total ions in the cell pairs of EDR divided by ions wasted from EDR every second as in Eq. (1) from [7].

$$MIRT_c = 0.5Q^{fc}(C_s^{fc} + C_s^{s})PRI/(Q^{co}C_s^{co}) \quad (1)$$

Concentrate from EDR with acid and anti-scalants operating with higher water recovery rate are required special disposal [11] for its high TDS and chemicals; concentrate from EDR without acid and anti-scalants can be discharged into WWTP [12] due to its low TDS and or reuse as water nutrient medium for bio-energy recovery in anaerobic bio-degradation [13,14]. Anti-scalant chemicals are synthesized. The disposal method for the synthesis chemical related concentrate streams are still in the research processes. The current practices of the disposal of synthesis chemical related concentrate are evaporation for the inland EDR and disposed off in seawater for the desalination near the sea. Due to new chemicals (anti-scalant, acids and biocides) are added into the sea in the every days or weeks, disposals of concentrates from EDR with acid and anti-scalant chemical into seawater have potential risks to both environments and humans [15]; these disposals are now called for reassessment by [16,17]. World Health Organization (WHO) also called for the protection of coastal ecosystems and groundwater aquifers from the intrusion from the concentrate disposals into the sea. Ref. [18] called for removing the hazardous constituents from concentrate of desalination before discharging into sea.

Moreover, [19] proved that there are *disadvantages* when EDR was operated with the *higher R* (>90%) in pilot scale testing by with high 42% feedwater (SO_4^{2-} 560.7 mg/l in 1829 mg/l TDS) without any pretreatment. The tests in Elyanow et al., 1981b included nine tests (#1, 2, 3, 4, 5, 5a, 5b, 5c, 6, 7) with different *R*; tests #1–5a was without any acid and without any SHMP; test 5b with the acid; and tests #5c–7 were with acids and SHMP. The results finds from [19] are summarized in Fig. 2(a–f). Fig. (2a) compares the metered *R* with calculated *R*. Fig. 2(b) compares the power consumption in different *R* with and with acid and/or SHMP. Fig. 2(c) shows current efficiency. Fig. 2(d) depicted the % demineralization in different tests. Fig. 2(e) compares power consumption per m^3 of product water

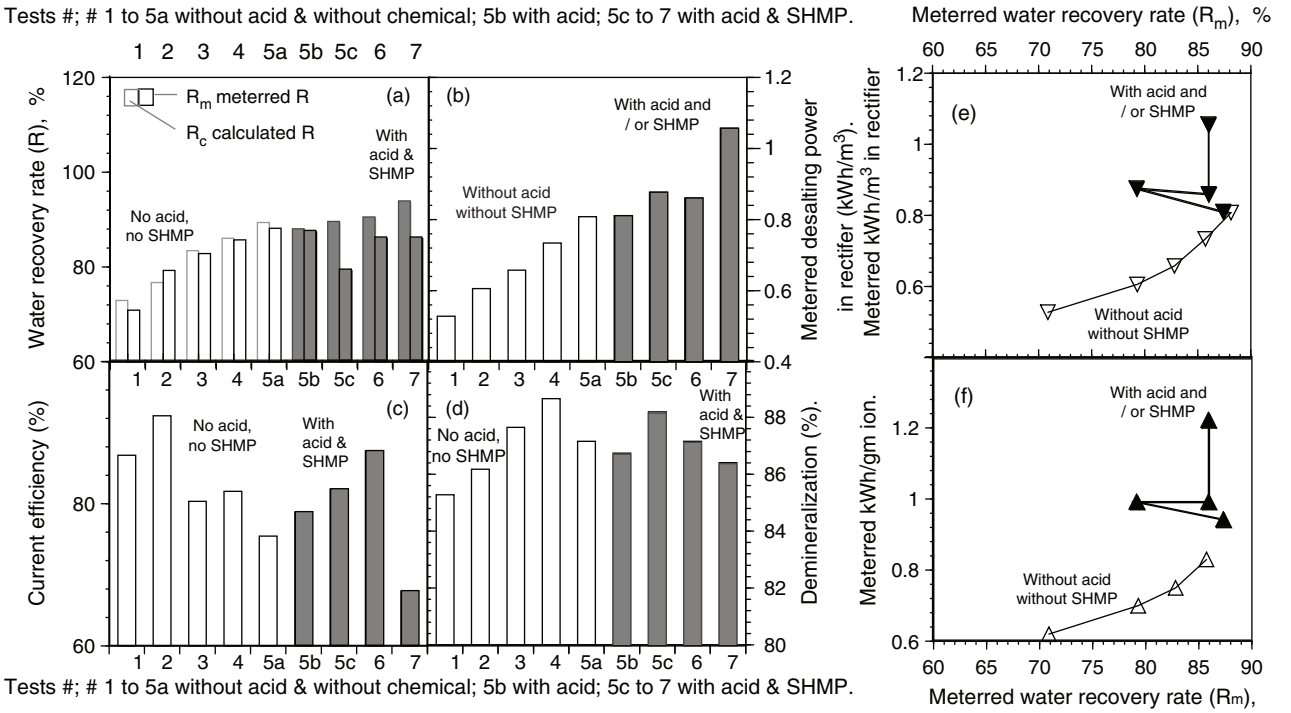

Fig. 2. (a) Tests in different water recovery rates (*R*) in with and without acid and/or SHMP addition; (b) tests in metered desalting power vs. different *R*; (c) current efficiency tests; (d) demineralization tests; (e) metered *R* vs. metered kWh/m^3 product water; (f) metered *R* vs. metered kWh/g ions. (Pointed markers and data, measured data, are referred from [23].)

with different *R*. Fig. 2(f) analyzes power consumption per gram of ions removed with different *R*. By increasing R_c from 73.0 to 89.4%, the hydraulic leaks are so small that R_m equals to R_c. When R_c is increased from 89.3 to 93.6 by adding acid and SHMP in concentrate stream to avoid sulfate fouling and carbonate precipitation, the hydraulic leaks are considerable that R_m is significantly smaller than R_c in Fig. 2(a). Fig. 2(b) shows the tests in metered power kW h/m^3 product water. One can conclude from Fig. 2(a) and (b) that there are disadvantages when the *R* increases from 89.3 to 93.6 in tests #5b–7 with the addition of acid and SHMP; these disadvantages are hydraulic leaks are significant and power consumption (kW h/m^3) increases. The optimal R_m 88.1 can be selected from Fig. 2(e) and (f) with the maximal *R* without any acid and chemical from tests #1–5a.

Due to its *hindering* the ions transport number in membrane, t_{im} and *enhancing* ions transport # in solution (t_{is}) in operation with the higher water recovery rate, *R*; due to its *enhancing* t_{im} and *hindering* t_{is} in membrane and in solution, respectively, in operation with optimal *R*, we hypothesize that the *energy consumption* and unit cost for desalting of the concentrate recycling system with the chemical may be higher than those with the optimal recycling ($MIRT_c$ < 130 min) and without chemical addition in concentrate stream.

Mathematical model incorporated with the experiment data is a powerful economical tool to depict and understand the inside science of water–environment system; a truthfully authenticated model allows engineers and scientists to enhance the understanding of the process performance that may advance the blueprint and the procedure principles to guarantee reliable treatment efficiencies. Since there is no mathematical model in literature for EDR, the *objectives* of this article are to develop *energy efficient* model based on theoretical LCD, concentration potential, and total area resistances of both membrane and solution; to verify LCD determination with lab data from Lee et al. (2006); to identify the most sensitive parameter in EDR with LCD; to fit, verify, and validate the model with six different pilot and filed data with five different characteristics of feedwater; and to analyze the desalting *energy consumption* relate to the requirement of acid and chemical addition and $MIRT_c$.

2. Model methods

2.1. Limitation current density (LCD) determination

Limiting current density (LCD) depends on ion concentration of feed into dilute stream (C_i^{fd}) [11]; electrochemical valence of the ions in feed of dilute stream (*z*); the hydrodynamics, flow channel geometry, spacer design (D_{is}/δ); transport numbers of ions in membrane and solution ($t_{im} - t_{is}$) [20] as follows:

$$i_{\text{lim.th}} = C_i^{\text{fd}} D_{is} zF/\{\delta(t_{im} - t_{is})\} \quad (2)$$

The ratio of D_{is}/δ is represented by the mass transfer coefficient (*k*) which can be correlated with Sherwood number in thin-channel length of practical interest as $k = 1.62(uD_{is}^2/d_h L_{\text{prac.tot}})^{0.33}$ in laminar flow (R_e < 2100) or as $k = 0.023u^{0.8}D_{is}^{0.672}/(d_h^{0.2}v^{0.47})$ in tubular flow, R_e > =2100 [6,21]. With these mass transfer coefficients, the theoretical LCD can be derived as Eq. (3) for laminar flow or Eq. (4) for tubular flow as follow:

$$i_{\text{lim.th}} = 1.62C_i^{\text{fd}} zF(uD_{is}^2)/\{d_h^{0.33} L_{\text{prac.tot}}{}^{0.33}(t_{im} - t_{is})\} \quad (3)$$

$$i_{\text{lim.th}} = 0.023C_i^{\text{fd}} zFu^{0.8}D_{is}^{067})/\{d_h^{0.2}v^{0.47}(t_{im} - t_{is})\} \quad (4)$$

LCD is calculated by the above Eqs. (3) and (4), and verified in Fig. 3(a) and validated in Fig. 3(b).

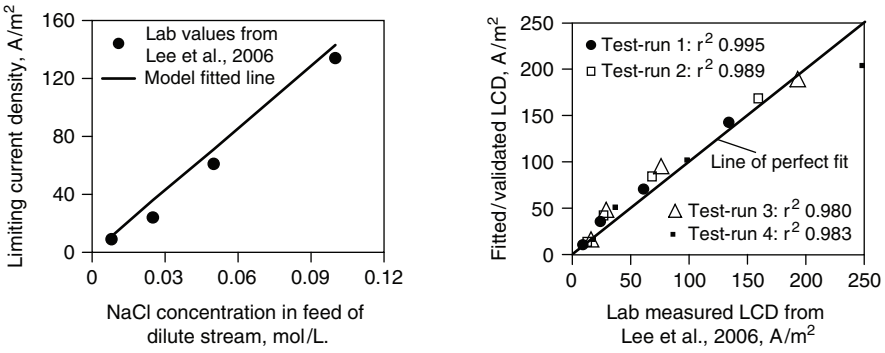

Fig. 3. (a) Comparison: limiting current density between lab vs. fitted model values; (b) Comparison: limiting current density (LCD) between lab vs. fitted/validated model value.

2.2. Specific energy consumption for ions desalinating in EDR

Specific energy consumption for desalinating ions in EDR is a function of cell geometry, feed water linear flow and electro-chemical characteristics, membrane properties [22], concentration potential [9], and *total area resistance* of both membrane and *solution* as follows:

$$E_s^{des} = [utk_{ce}\alpha(C_s^{fd} - C_s^{d})^2 z^2 F^2 / (\zeta^2 L_{prac.tot})] \\ [tk_{ce} / \{\Lambda(C_s^{fd} - C_s^{d})\} + (\rho_A + \rho_C + \rho_{Solu})]F_{\Delta\psi} \quad (5)$$

$$F_{\Delta\psi} = \ln((C_s^{fc} + C_s^{c})\gamma^{c} / (C_s^{fd} + C_s^{d})\gamma^{d}) \quad (6)$$

2.3. Mass balance diagram in EDR

The mass balance diagram in Fig. 4 was used to calculate the concentrate recirculation flow rate and the ions concentration recycled into inlet of concentration stream. The equations used in the model are summarized in Table 1.

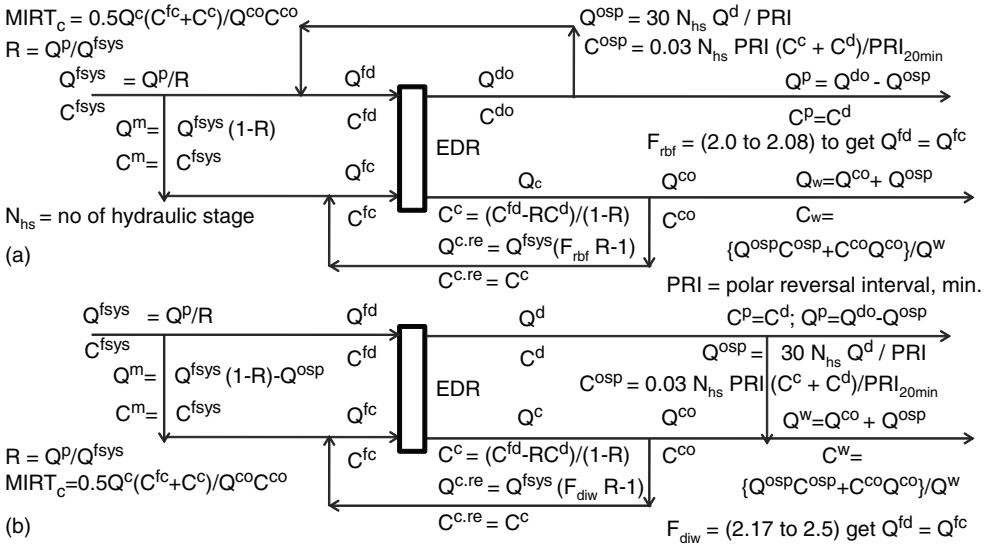

Fig. 4. Mass balance diagram of EDR. (a) Off-spec product (osp) recycle back into feed; (b) osp wastes into wastes line.

Table 1
More equations used in cost model

Equations used in model		Reference
TDS concentration in concentrate out, keq/m^3 = $C_s^c = (C_s^{fd} - RC_s^d)/(1-R)$		[22]
TDS concentration feed to concentrate, keq/m^3 = $C_s^{fc} = (C_s^{fd}(1-R)/R) + (C_s^c(2R-1)/R)$		[22]
Practical limiting current density, A/m^2 = $i_{prac} = s\, i_{emplim.th}$		[22]
$g = [\{1\} + \{\Lambda(\rho_A + \rho_C + \rho_{Solu})(C_s^{fd} - C_s^{d})/tk_{ce}\}]zFC_s^d utk_{ce}\alpha$		
$h = [\{(C_s^d/C_s^c) + 1 + (\Lambda C_s^d(\rho_A + \rho_C + \rho_{Solu})/tk_{ce})\}si_{lim}\beta\zeta]$		
$L_{prac.tot}$, $m = g/h$		
Ionic strength in solution, keq/m^3 = I_{stre} = 0.5 Sum $((z_i)^2[C_i])$		
Activity coefficient in dilute = $\gamma^d = \exp(-0.509Z_i^2(I^{0.5}/(1+(I^{0.5}))))$	if $I < 0.1$	[28]
Activity coefficient in dilute = $\gamma^d = \exp(-0.509Z_i^2(I^{0.5}/(1+(I^{0.5})) - 0.2I))$	if $I < 0.5$	[28]
Activity coefficient = $\gamma^c = \exp[-0.509\, Z_i^2\{I^{0.5}/(1 + 0.3287\, a(I^{0.5})\} + bI]$	if $I < 1$	[28,29]
Cell pair voltage drop, $V = U_{cp} = tk_{ce}[(1/C_s^c) + (1/C_s^d) + \{\Lambda(\rho_A + \rho_C + \rho_{Solu})/tk_{ce}\}]i_{prac}\beta/(\Lambda)$		
Total membrane surface area, $m^2 = 2N_{ce}A_{prac} = gg/h$		[22]
$gg = [\{1\} + \{\Lambda(\rho_A + \rho_C + \rho_{Solu})(C_s^{fd} - C_s^{d})/tk_{ce}\}]\, zFC_s^dQ^d$		
Number of cell pair = $N_{cp} = Q^d/(wtk_{ce}u\ \alpha)$		
Total current through one cell pair, $A = I_{ce} = zFQ^d(C_s^{fd} - C_s^{d})/(\zeta N_{cp})$		[22,30]
Total current through all cell pair, $A = I_{tot} = zFQ^d(C_s^{fd} - C_s^{d})/(\zeta)$		

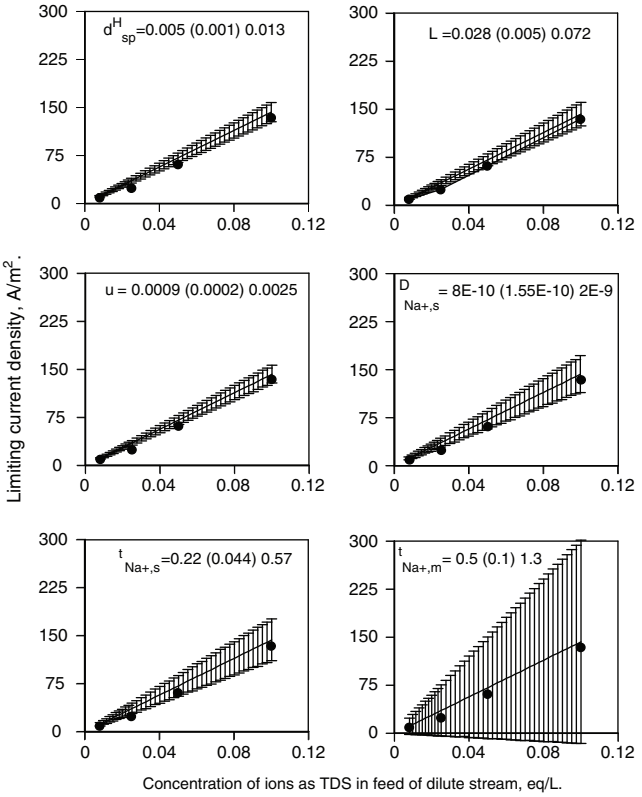

Fig. 5. Sensitivity analysis of limiting current density to the modeling parameter. Pointed markers are lab data from Lee et al. 2006 or [22].

2.4. Sensitivity analysis

A sensitivity analysis exercise was conducted to identify the most sensitive parameters in the LCD (Eq. 3), with Test-run 1: u 0.017 m/s. For each of the six parameters (d_h, L, u, D_{is}, t_{is}, t_{im}), nine values were selected over a typical range, and nine simulations were run at each of those values to generate nine LCD profiles. These profiles were combined to generate a mean with a spread of one standard deviation. A compilation of these mean profiles for each of six parameters is presented in Fig. 5, along with the measured LCD from Test-run 1 of [20]. NaCl was used as model salt ions in [20]' experiment. These plots indicate that the transport number of ions (Na^+) in membrane $t_{Na^+,m}$ to be highly sensitive, followed by transport number of ions (Na^+) in solution (Na^+), to a lesser extent.

2.5. Model input parameters

Model input parameters include feedwater characteristics, common parameters for all model-runs, specific parameters for each model-run. Feedwater characteristics contain three different types from five different groundwater sources, are summarized in Table 2. The three different types of feedwater are high waters, high NaCl water, and common simple water. Nine Test-runs of Pilot scale data from [19] in column 1 of Table 2 are used to fit the cost efficient model. [23] stated 18 Test-runs with two different types of anion membrane in

Table 2
Water characteristics, data, membrane types from literatures used in model

Different characteristic feedwaters/Reference	Fitting	Verifying		Validating		
	19	23		24	25, 26	27
Column number	1	2	3	4	5	6
Test-run	9	9	9	1	1	1
Na^+, eq/l	0.0103	0.0574	0.0574	0.010	0.0041	0.0060
Ca^{2+}, eq/l	0.0115	0.0075	0.0075	0.008	0.0070	0.0090
Mg^{2+}, eq/l	0.0057	0.0034	0.0034	0.006	0.0043	
K^+, eq/l		0.0001	0.0001		0.0001	0.0003
Cl^-, eq/l	0.0128	0.0586	0.0586	0.001	0.0016	0.0082
HCO_3^-, eq/l	0.0037	0.0011	0.0011	0.009	0.0044	0.0031
SO_4^{2-}, eq/l	0.0113	0.0003	0.0003	0.015	0.0100	0.0079
NO_3^-, eq/l					0.0003	0.0002
Sum of ions, eq/l	0.0276	0.0642	0.0642	0.0247	0.0159	0.0172
TDS gravimetric, eq/l	0.0274	0.0634	0.0634	0.0250	0.0156	0.0199
Conductivity, mS/cm	2540					
pH	7.48			7.6	7.2	
Type of spacer		Ionics' Mark III-4			Mark IV	
Member–anion	204SXZL	103PZL	204SXZL	Aquamite V	2020	V-M

Aromatic 103PZL anion membrane, aliphatic 204SXZL anion membrane

Table 3
Model inputs—common parameters for all model-runs

Ion (Na^+) transfer # in membrane, $t_{Na^+,m}$	0.90	[31,32]
Ion (K^+) transfer # in membrane, $t_{K^+,m}$	0.98	[33]
Ion (K^+) transfer # in solution, $t_{K^+,s}$	0.5	[34]
Equivalent conductance of solution at 20 °C, Λ	11.7422	S m^2/keq [35]
Thickness of cell chamber, tk_{ce}	0.00065	m; [30]
Faraday constant, F	96485300	As/keq
Total area of membrane resistance, $\rho_A + \rho_C$	0.0007	Ω m^2; [22]
Safety factor, s	0.7	[5]
Current utilization, z	0.9	[22]
Effective width of cell, w	0.42	m; [22]
Effective length of flow path per stack, L_{st}	0.725	m; [22]
Distance between two rods in spacer, l_{sp}	0.002	m; [36]
$k_{Na^+}=1.62((uD^2_{Na^+})/(d_hL))^{0.33}$	1.5E−0.5	m/s; [21]′ equation
$k_{Mg^+}=1.62((uD^2_{Mg^+})/(d_hL))^{0.33}$	9.7E−0.6	m/s; [21]′ equation
$k_{K^+}=1.62((uD^2_{K^+})/(d_hL))^{0.33}$	1.9E−0.5	m/s; [21]′ equation
Typical values for mass transfer coefficient (k) 10^{-5} to 10^{-3} m/s [11]		

columns 2 and 3 of Table 2. Data from [23]′ pilot scale nine Test-runs with aromatic 103PZL anion membrane are used to verify the cost efficient model. The remaining data from [23]′ nine Test-runs with aliphatic 204SXZL anion membrane are used to validate the cost efficient model. Moreover, data from another four field Test-runs from [24–27] are also used in validate the model.

Tables 3 and 4 show common parameters for all model-runs and specific parameters for each model-run. Common parameters for all model-runs include literature verified parameters such as ion Na^+ transport number through membrane ($t_{Na^+,m}$), ion Ca^{2+} transport number through membrane ($t_{Ca^{++},m}$), ion K^+ transport number in solution ($t_{K^+,s}$), equivalent conductance of solution at 20 °C, thickness and efficient width of cell channel, total area resistance of membranes, safety factors, efficiency of current utilization, effectiveness of flow path per stack. The calculated mass transfer constants of ions Na^+, Ca^+, Mg^+, and K^+ with the literature equations are also included in Table 3 as common parameters for all model.

Table 4 includes operation parameters (flow rates, water recovery rates, linear velocity in cell); water characteristics (TDS in feedwater and in product); and controlling parameter (polar reversal interval) for each model-run due to their difference in each test-run from literature.

2.6. Energy efficient model fitting, verification, and validation

The model is fitted with *nine* Test-run measured desalting energy data from pilot scale demonstration [19] with r^2 0.913 in Fig. 6(a) with the high SO_4^{2-} analogous to Alamogordo groundwater in CR61 CZL-386 and AR204 SXZL membranes. The model is also verified with *nine* Test-run measured desalting energy data from pilot scale demonstration [23] with r^2 0.900 in Fig. 6(b) with the high NaCl analogous to Virginia Beach, Virginia, water in CR61 CZL–386 and aromatic 103 PZL membranes. The model is also validated with another *nine* Test-run measured desalting energy data from pilot scale demonstration [23] with r^2 0.975 in Fig. 6(c) with the high NaCl analogous to Virginia Beach, Virginia, water in CR61 CZL–386 and aliphatic 204 SXZL membranes. This validation also includes another four sets of measured data from [24–27]. The overall competences of model are shown in Fig. 6(d) with overall r^2 0.916.

With the same procedures of fitting, verification, and validation of the model, the model parameters ($t_{Ca^{++},m}$, $t_{Mg^{++},m}$, $t_{Na^+,s}$, $t_{Ca^+,s}$, $t_{Mg^{++},s}$) are fitted, verified, and validated, with overall 30 set of measured pilot and filed scales TDS data in Fig. 7(a)–(c) with r^2 0.912, 0.993, 0.996, respectively. The overall competences of model fitting parameter are shown in Fig. 7(d) with overall r^2 0.987 in minimum three different types of membrane and six different sources. The fitted, verified, validated parameters are summarized in Table 5.

2.7. Numbers of unknown parameters, and number of fitting model

The numbers of unknown fitted by model are seven parameters that are fitted, verified, and validated in thirty model-runs. The numbers of unknown parameters and the number of model-runs are justified.

Table 4
Specific parameters for model inputs; model output, and model finding

Model input-specific parameters for model-runs																														
MR #	1	2	3	4	5	6	7	8	9	10	11	12	13	14	15	16	17	18	19	20	21	22	23	24	25	26	27	28	29	30
Reference				[19]													[23]											[24]	[25,26]	[27]
Q^p, m^3/d	102	101	103	101	99.7	96.3	86.3	87.2	87.4	99.7	97.1	99.5	95.5	94.8	90.5	101	99.4	95.8	99.5	98.5	98.9	97.0	96.2	92.4	103	101	100	1929	43.8	105
R_{PPf}	0.71	0.79	0.83	0.86	0.88	0.87	0.89	0.90	0.94	0.74	0.79	0.83	0.87	0.90	0.92	0.84	0.90	0.93	0.73	0.79	0.84	0.87	0.91	0.93	0.84	0.92	0.94	0.84	0.887	0.91
C_s^{fd}, eq/L		0.0276;		MR # 1–9 are to fit the model						0.0642;		MR# 10–18 are to verify the model							0.0642;		MR# 19–30 are to verify the model							0.025	0.0016	0.017
C_s^d, eq/L					0.0041;									0.0064;									0.0064;					0.007	0.005	0.002
u, m/s	0.08	0.07	0.08	0.07	0.07	0.06	0.06	0.06	0.06	0.08	0.07	0.07	0.07	0.07	0.07	0.07	0.07	0.08	0.07	0.07	0.07	0.07	0.07	0.07	0.08	0.07	0.07	0.15	0.11	0.15
				(0.075 m/s Lee et al., 2002; 0.0111 m/s Tsia and P, 2005)																										
Polar reversal interval, min												20 min					30 min				20 min					30 min		15 min	
Model outputs from model-runs																														
E_s, kWh/m^3	0.62	0.77	0.79	0.86	0.94	0.89	0.92	0.99	1.31	1.95	2.23	2.30	2.46	2.76	3.04	2.27	2.72	3.26	1.85	2.17	2.28	2.47	2.94	3.32	2.24	2.93	3.56	0.42	0.351	0.62
Model findings from model-runs																														
ρ_{sol}, Ω m^2 (10^3)	4.78	4.71	4.52	4.62	4.70	5.98	5.46	5.72	5.45	4.66	4.83	4.60	4.89	4.92	5.30	4.40	4.46	4.71	4.69	4.72	4.65	4.78	4.80	5.12	4.23	4.32	5.09	2.24	3.56	2.78
MIRT, min	40	66	84	106	133	127	150	166	266	53	73	96	131	190	243	143	270	402	52	75	105	133	221	282	149	325	471	173		

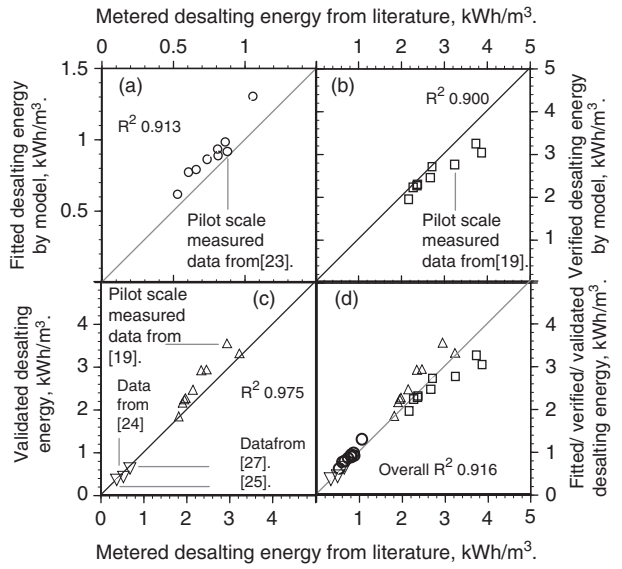

Fig. 6. Comparison of model values with metered desalting energy data. (a) model fitting; (b) model verification; (c) model validation; (d) overall competences.

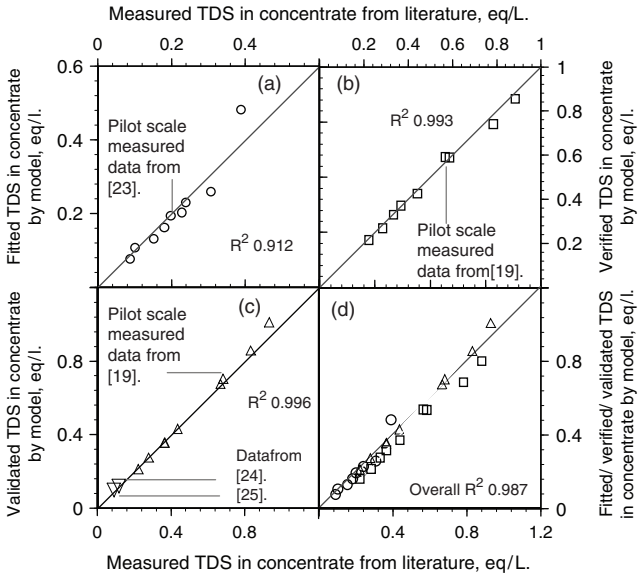

Fig. 7. Comparison of Model values with measured TDS in concentrate wasted. (a) model fitting; (b) model verification; (c) model validation; (d) overall competences.

3. Results

3.1. Results in verification and validation of limitation current density

LCD values predicted by the model were compared against the experiment data from Lee et al., 2006 to verify and validate the model. As shown in Fig. 3(a), model predictions using the parameters established in this study closely followed the temporal trend in the measured LCD data from Test-run 1, which has u 0.017 m/s. Measured data from Test-runs 2, 3 and 4 were used to further validate the model. The variable which distinguishes Test-runs 2, 3 and 4 from each other and from Test-run 1 is linear velocity of solution. Fig. 3(b) shows the agreement between the LCD values predicted by the model and the measured COD values from the four Test-runs. The agreement between the predicted and measured LCD values was statistically significant ($p < 0.011$), individually for the four test-runs (with r^2 0.995, 0.989, 0.980, and 0.983, respectively) as well as for the four Test-runs together (with overall r^2 0.966 at $p < 0.001$). This agreement validates the modeling approach as well as the three model parameters established in this study.

Table 5
Model fitted, verified, validated parameters

Ion (Ca^{++}) transfer # in membrane, $t_{Ca^{++},m}$	0.95
Ion (Mg^{++}) transfer # in membrane, $t_{Mg^{++},m}$	0.95
Ion (Na^{+}) transfer # in solution, $t_{Na^{+},m}$	0.10
Ion (Ca^{++}) transfer # in solution, $t_{Ca^{++},m}$	0.10
Ion (Mg^{++}) transfer # in solution, $t_{Mg^{++},m}$	0.10

3.2. Results from energy efficient model

The results from energy efficient model are showed in Table 4.

3.3 Modeling finding

The area resistances of solutions for 27 model-runs are plotted in Fig. 8(a)–(c) against the $MIRT_c$. Fig. 8(a) compares the area resistances between the solutions with and without acids and anti-scalants. Fig. 8(b) compares the area resistances of the solutions, without acids and without anti-scalants between 20 and 30 min polar reversal interval of EDR. Fig. 8(c) compares the area resistances of the solutions, with acids and with anti-scalants (SHMP) between 20 and 30 min polar reversal interval of EDR. The relationship between area resistances of solutions and desalting energy in EDR are found from the model-runs that are shown in Fig. 8(d–f). Fig. 8(d) compares the desalting energies between the solutions with and without acids and anti-scalants. Fig. 8(e) compares the desalting energies of the solutions, without acids and without anti-scalants between 20 and 30 min polar reversal interval of EDR. Fig. 8(f)

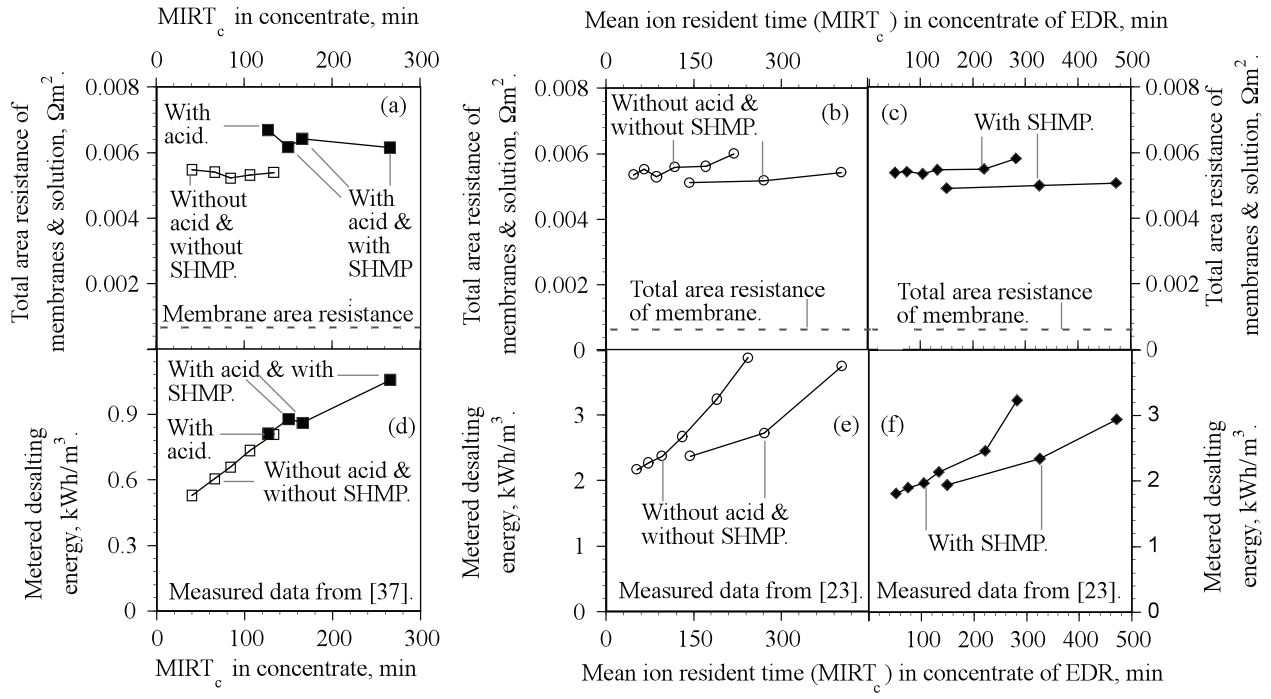

Fig. 8. Area resistances of solutions vs. MIRT$_c$ in (a)–(c); relation of area resistances of solutions with metered desalting power vs. MIRT$_c$ in (d)–(f).

compares the desalting energies of the solutions, with acids and with anti-scalants (SHMP) between 20 and 30 min polar reversal interval of EDR.

4. Discussions

The predicted desalting energy is slightly over fitted (Fig. 6a) and over validated by model (Fig. 6c) while fitted and validated desalting energy results are comparing with the measured data from [19,23]. However, the verified desalting energy is slightly under estimated by model while comparing the measured desalting energy values with modeling results in Fig. 6(b). The degrees of matching in desalting energy data are acceptable with overall r^2 0.916 (Fig. 6d) in such a complicated nature of EDR. The predicted TDS values are perfectly matched with the measured data in fitting (r^2 0.912 in Fig. 7a), verifying (r^2 0.993 in Fig. 7b), and validating (r^2 0.996 in (Fig. 7c).The goodness of matching in desalting energy data are acceptable with overall r^2 0.987 (Fig. 7d) in such a complicated nature of EDR.

4.1. Discussions in area resistance of solutions

The values of area resistances of solutions in EDR are generated from model. The generated values from model-runs 1 to 9 (for solutions from [19]), 10 to 18 (for solutions from [23] with aromatic 103PZL anion membrane), and 19 to 27 (for solutions from [23] with aliphatic 204 SXZL anion membrane) are plotted in Fig. 8(a–c) against the MIRT$_c$. The model data shows that if MIRT$_c$ increases, area resistances of solution increases in Fig. 8(b and c); then the required desalting energies increases due to the increases of area resistances of solution in EDR (Fig. 8d–f). Solutions containing the acids and anti-scaltant (SHMP) have the higher area resistances than solutions without acids and SHMP (Fig. 8a). Solutions containing the acids have the higher desalting energy consumption (0.811 kWh/m^3) than 0.785 kWh/m^3 in solutions without acids [19]'s pilot scale demonstration data) in the same of feedwaters and in the same of water recovery rate of 87.4% where there is no water leak detected. Table 6 shows that, there is no water leak if EDR is operated MIRT$_c$ < 130 min; more than that 130 min MIRT$_c$, the pilot scale data shows water leaks. From the analysis in Table 6, there is 3.2–31% desalting energy saving if EDR is operated at MIRT$_c$ < 130 min at which condition acids and SHMP is not required to add in concentrate and there is no water leaks [19]. The will be more cost saving if the cost of acids is included. Although, the operations in 30 min PRI has the higher MIRT$_c$, the solutions in 30 min PRI has lesser area resistance than the solutions in 20 min PRI in both cases of the solutions with (Fig. 8b) and without (Fig. 8c) acids and anti-scalants. Due to these lesser area resistances in the solutions of 30 min PRI, the 30 min PRI operations requires the lesser desalting energies than the 20 min PRI operations in both cases of the solutions with (Fig. 8f) and without (Fig. 8e) acids and anti-scalants.

Table 6
Comparison of operations with and without acid and anti-scalant

Operation with acid and/or SHMP				Operation without acid and without SHMP					
$MIRT_c$, min	ρ_{solu}, Ω m²	Analyzed *R*%	Metered *R*%	Metered desalting energy			$MIRT_c$, min	ρ_{solu}, Ω m²	Energy saving, %
				kW h/m³	Leak?	kW h/m³	Model predicted		Calculated
Model predicted		Elyanow et al., 1981b				Interpolated[1]			
127	0.0067	87.72	87.4	0.811*	No leak	0.785	112	0.0053	3.2
150	0.0062	89.28	79.23	0.877**	Water	0.604	66	0.0054	31
166	0.0064	90.21	86.01	0.861**	Leak	0.743	109	0.0053	14
266	0.0062	93.58	86.00	1.057**	Leak	0.743	109	0.0053	30

[1] Interpolated based on Elyanow et al., 1981b pilot scale data; Wo = without; *R* = water recovery rate; w = with;
$\rho_{solution}$ = area resistance of solition;
*adding acid only in concentrate; ** both acid and SHMP are added in concentrate

5. Conclusion

A new model is developed, verified, and validated. Five parameters ($t_{Ca^{++},m}$, $t_{Mg^{++},m}$, $t_{Na^{+},s}$, $t_{Ca^{++},s}$, $t_{Mg^{++},s}$) are generated from 30 model-runs. A new model and the measured data from literature point out there is a new operation for the EDR. This new operation is recommended for EDR to operate at $MIRT_c$ < 130 min. At $MIRT_c$ < 130min, there are no water leakage and no requirement to add acid and SHMP, and solutions inside EDR has the low area resistance of solutions. By operating EDR at $MIRT_c$ < 130min, desalting energy consumption are found to be reduced from 3.2% to 31% in [19] pilot scale study.

Acknowledgement

We thank and appreciate the funding agency the Office of Naval Research (Contract # N00014-08-1-0304) from the USA.

Symbols

C_s^d — Concentration of total ions as TDS in outlet of dilute stream, keq/m³
C_s^{fd} — Concentration of total ions as TDS in feed into dilute of EDR, keq/m³
C_s^c — Concentration of TDS in outlet of concentrate stream, keq/m³
C_s^{co} — Concentration of TDS in outlet of concentrate stream, keq/m³
C_s^{fc} — Total ions as TDS in inlet of concentrate feed stream inlet, keq/m³
D_{is} — Diffusion coefficient of ion in solution, m²/s
d_{sp}^H — d^H = Equivalent hydraulic diameter of spacer, m
E_s^{des} — Specific power consumption for desalting ions in cell, kW h/m³
F — Faraday constant, A s/keq.
$F_{\Delta\psi}$ — Factor for concentrations potential
$i_{lim.th}$ — Limiting current density from theory, A/m²
$i_{lim.prac}$ — Practical design current density, A/m²
I_{ce} — Total current through one cell pair, A
$I_{stre.f}$ — Ionic strength of solution in feed stream to EDR, mol/l
$I_{stre.c}$ — Ionic strength of solution in outlet of concentrate stream in EDR, mol/l
$I_{stre.d}$ — Ionic strength of solution in dilute stream to EDR, mol/l
I_{tot} — Total current through all the cell pair, A
l_{sp} — Distance between two rods in spacers, m
k — Ion mass transfer coefficient from dilute into concentrate, unit-less
$L_{prac.tot}$ — L = Total length of practical flow path in the stacks, m
$MIRT_c$ — Mean ions retention time in concentrate and recirculation into concentrate of EDR, min
$2N_{ce}A_{prac} = A_{mem}$ — Total membrane area, m²
N_{cp} — Total number of cell pair, no unit
N_{st} — Number of stacks in series, no unit
PRI — Polar reversal interval in EDR, min
Q^{co} — Flow rate out from concentrate stream after recycling point, m³/s
$Q^{conc.re}$ — Flow rate in concentrate recycle stream, m³/s
$Q^{d.prac}$ — Flow rate in dilute stream out from EDR as product, m³/s

Q^{fc} — Feed flow rate in concentrate stream, m^3/s
Q^{fd} — Flow rate feed in inlet of dilute stream, m^3/s
Q^{fsys} — Flow rate in feed stream into EDR system before make-up stream, m^3/s
Q^{m} — Flow rate in make-up stream, m^3/s
$Q^{thr\ cell}$ — Flow rate through cell stack in concentrate & dilute compartments, m^3/s
Q^{w} — Flow rate in waste discharged from EDR every second, m^3/s
R_e — Reynolds number, unit-less
S_c — Schmidt numbers, unit-less = ν/D_{is}
S_h — Sherwood number, unit less
tk_{ce} — Thickness of cell chamber, m
u — Linear flow velocity, depending on type of spacer, m/s
U_{cp} — Cell pair voltage drop, V
U_{st} — Potential drop per stack, V
z — Electrochemical valence of ion in solution, no unit

Greeks

α — Volume factor, no unit
β — Area factor accounting for shadow effect, no unit
ζ — Efficiency of current utilization, no unit
Λ — Equivalent conductance of solution at 20 °C, S m^2/keq.
$\rho_A + \rho_C$ — Total area of resistance in anion & cation membranes, ohm m^2
ρ_{Solu} — Total area of resistance of solution in both sides of membranes, ohm m^2
γ^c — Activity coefficient in solution flowing in concentrate stream of EDR
γ^d — Activity coefficient in the solution flowing in dilute stream of EDR
γ^f — Activity coefficient of solution in feed stream, no unit
δ — Thickness of the boundary layer, m
ν — Kinematic viscosity, m^2/s

References

[1] F.H. Meller, Electro-dialysis (ED) and Electro-dialysis Reversal (EDR) Technology, Ionics Inc., Watertown, MA. 1984.
[2] W.E. Katz, The electro-dialysis reversal (EDR) process, Desalination, 28 (1979) 31–40.
[3] E. Reahl, Reclaiming reverse osmosis blowdown with electrodialysis reversal, Desalination, 78 (1990) 77–89.
[4] M. Turek, J. Was and P. Dydo, Brackish water desalination in RO-single pass EDR system, Desal. Water Treat., 7 (2009) 263–266.
[5] AWWA Manual of Water Supply Practices- M38, Electrodialysis and Electro-dialysis Reversal, American Water Works Association, Denver, CO, 1st ed., 1995.
[6] Y. Tanaka, Ion exchange membranes: fundamentals and applications, in: Membrane Science and Technology Series 12, Elsevier, London, 2007.
[7] M.T. Myint, A. Ghassemi and N. Nirmalakhandan, Low Energy/cost Desalination: Low Dose & Low Mean Ion Resident Time in Concentrate stream of Electro-dialysis Reversal. In 7th IWA leading-edge conference on water and wastewater technologies April 2–4, 2010 Phoenix, the USA. In Press in Wat. Sci. Technol., Reference No: WST-WSTWS-EM10818R1.
[8] M. Arda, E. Orhan, O. Arar, M. Yuksel and N. Kabay, Removal of fluoride from geothermal water by electro-dialysis (ED), Sep. Sci. Technol., 44 (4) (2009) 841–853.
[9] W.S.W. Ho and K.K. Sirkar, Membrane Handbook, Van Nostrand, Reinhold, New York (1992).
[10] A. Kitamoto and Y. Takashima, Transfer rates in electrodialysis with ion exchange membrames, Desalination, 9 (1971) 51–87.
[11] T.A. Davis, J.D. Genders and D. Pletcher, A First Course in Ion Permeable Membranes. Hants, England: The Electrochemical Consulancy (1997).
[12] A.M.O. Mohamed, M. Maraqa and J.A. Handhaly, Impact of land disposal of reject brine from desalination plants on soil or groundwater, Desalination, 182 (1–3) (2005) 411–433.
[13] Y.-G. Lim, C. Niwa, N. Nagao and T. Toda, Solubilization and methanogenesis of blue mussels in saline mesophilic anaerobic biodegradation, Int. Biodet. Biodegrad., 61 (3) (2008) 251–260.
[14] S. Alkaabi, P.J. van Geel and M.A. Warith, Effect of saline water and sludge addition on biodegradation of municipal solid waste in bioreactor landfills, Waste Manage. Res., 27 (1) (2009) 59–69.
[15] P. Chelme-Ayala, D.W. Smith and M.G. El-Din, Membrane concentrate management options: a comprehensive critical review, Canada J. Civil Eng., 36 (6) 1107–1119.
[16] S. Lattemann and T. Hopner, Environmental impact and impact assessment of seawater desalination, Desalination, 220 (2008)1–15.
[17] H. A. Qdais, Environmental impacts of the mega desalination project: the Red-Dead Sea conveyor, Desalination, 220 (2008) 16–23.
[18] A. Hashim and M. Hajjaj, Impact of desalination plants fluid effluents on the integrity of sweater, with the Arabian Gulf in perspective, Desalination, 182 (2005) 373–393.
[19] D. Elyanow, E. Sieveka and J. Mahoney, The determination of super-saturation limits in an EDR unit with aliphatic anion membranes. Ninth Annual Conference and International Trade Fair of the National Water Supply Improvement Association, Volume II. May 31 – June 4. (1981).
[20] H.-J. Lee, H. Strathmann and S.-H. Moon, Determination of the limiting current density in electrodialysis desalination as an empirical function of linear velocity. Desalination, 190 (2006) 43–50.
[21] M.C. Porter, Concentration polarization with membrane ultrafiltration, Ind. Eng. Chem. Prod. Res. Develop., 11 (3) (1972) 234–248.
[22] H.-J. Lee, F. Sarfert, H. Strathmann and S-H. Moon, Design of an electro-dialysis desalination plant, Desalination, 142 (3) (2002) 267–286.
[23] D. Elynaow, R.G. Parent and J.R. Mahoney, Parametric tests of an electrodialysis reversal (EDR) system with aliphatic anion membranes, Desalination, 38 (1981) 549–565.
[24] R.C. Harries, D. Elyanow, D.N. Heshka and K.L. Fischer, Desalination of brackish groundwater for a prairie community using electro-dialysis reversal, Desalination, 84 (1991) 109–121.
[25] J. Passanisi, J. Persechino and T.L. Reynolds, Technologies used at a brackish water reclamation facility, in: AWWA Annual Conference, The America Water Works Association, 2000.
[26] T.K. Reynolds and F. Leitz, Two years of operating experience at the port Hueneme brackish water reclamation demonstration facility, in: AWWA: Water Desalting Planning Guide for Water Utilities, America Water Works Association, 2004.
[27] H.C. Valcour Jr., Recent applications of EDR, in: Conference Proceedings: Second World Congress on Desalination and Water Re-use, Bermuda, Nov. 17–22 (1985).
[28] K. Al-Anezi and N. Hilal, Scale formation in desalination plants: effect of carbon dioxide solubility, Desalination, 204 (2007) 385–402.
[29] D.L. Parkhurst, Ion-association models and mean activity coefficients of various salts, in: D.C. Melchior and R.L. Bassett,

eds., Chemical Modeling of Aqueous Systems II, American Chemical Society, Washington, DC, 1990, pp. 30–36.
[30] P. Tsiakis and G. Papageorgiou, Optimal design of an electrodialysis brackish water desalination plant, Desalination, 173 (2005) 173–186.
[31] D. Elyanow, E. Sieveka and J. Mahoney, The determination of super-saturation limits in an EDR unit with aliphatic anion membranes. Ninth Annual Conference and International Trade Fair of the National Water Supply Improvement, (1981).
[32] B.V. der Bruggen, A. Koninckx and C. Vandecasteele, Separation of monovalent and divalent ions from aqueous solution by electrodialysis and nanofiltration, Water Res., 38 (5) (2004) 1347–1353.
[33] A. Lehmani, P. Turq, M. Périé, J. Périé and J.-P. Simonin, Ion transport in Nafion 117® membrane, J. Electroanal. Chem., 428 (1997) 81–89.
[34] V.I. Zabolotskii, N.P. Gnusin, V.V. Nikonenko and M.K. Urtenov, Convective–diffusive model of electro-dialytic desalination, Distribution of the concentration and current density, Sov. Electrochem., 21 (3) (1985) 269–275.
[35] K.S. Spiegler, Polarization at ion exchange membrane-solution interface, Desalination, 9 (1971) 367–385.
[36] R.A. Robinson and R.H. Stokes, Electrolyte Solutions. Dover Publications, Inc., Mineola, New York, 2002.
[37] H. Strathmann, Ion-exchange Membrane Separation Processes, Elsevier, Amsterdam, 2004.